coatings

MDPI

*Article*

# Sorption of Fulvic Acids onto Titanium Dioxide Nanoparticles Extracted from Commercial Sunscreens: ToF-SIMS and High-Dimensional Data Analysis

**Narjes Tayyebi Sabet Khomami [1], Alexander Welle [2,3], Stefan Kunz [1] and Allan Philippe [1,*]**

[1] Institute for Environmental Sciences (iES), Koblenz-Landau University, Fortstrasse 7, 76829 Landau, Germany; tayyebi@uni-landau.de (N.T.S.K.); stkunz@uni-landau.de (S.K.)
[2] Institute of Functional Interfaces, Karlsruhe Institute of Technology (KIT), 76344 Karlsruhe, Germany; alexander.welle@kit.edu
[3] Karlsruhe Nano Micro Facility (KNMFi), Karlsruhe Institute of Technology (KIT), 76344 Karlsruhe, Germany
* Correspondence: philippe@uni-landau.de

**Abstract:** Titanium dioxide nanoparticles (n-$TiO_2$) are common ingredients of sunscreens and are often released into surface waters during usage. Once released, the surface chemistry of n-$TiO_2$ changes by interacting with dissolved organic matter (DOM). In previous studies, these interactions were investigated using model n-$TiO_2$ and; therefore, do not account for the complex composition of the coating of n-$TiO_2$ aged in sunscreens. Taking advantage of a mild extraction method to provide more realistic nanoparticles, we investigated the potentials of time of flight-secondary ion mass spectrometry (ToF-SIMS) combined with high-dimensional data analysis to characterize the sorption of fulvic acids, as a model for DOM, on titanium dioxide nanoparticles extracted from ten different commercial sunscreens (n-$TiO_2$ ⊂ sunscreen). Clustering analysis confirmed the ability of ToF-SIMS to detect the sorption of fulvic acids. Moreover, a unique sorption pattern was recognized for each n-$TiO_2$ ⊂ sunscreen, which implied different fractionation of fulvic acids based on the initial specifications of nanoparticles, e.g., size, coating, etc. Furthermore, random forest was used to extract the most important fragments for predicting the presence of fulvic acids on the surface of n-$TiO_2$ ⊂ sunscreen. Finally, we evaluate the potential of ToF-SIMS for characterizing the sorption layer.

**Keywords:** sunscreen; extraction; $TiO_2$ nanoparticles; ToF-SIMS; high-dimensional data analysis; random forest



**Citation:** Tayyebi Sabet Khomami, N.; Welle, A.; Kunz, S.; Philippe, A. Sorption of Fulvic Acids onto Titanium Dioxide Nanoparticles Extracted from Commercial Sunscreens: ToF-SIMS and High-Dimensional Data Analysis. *Coatings* **2022**, *12*, 335. https://doi.org/10.3390/coatings12030335

Academic Editor: Alexander Tolstoguzov

Received: 2 February 2022
Accepted: 28 February 2022
Published: 3 March 2022



## 1. Introduction

Nanoparticulate inorganic UV filters are being increasingly used in sunscreens as an alternative to organic UV filters with reported detrimental effects on aqueous environments [1]. Among inorganic UV filters, titanium dioxide nanoparticles (n-$TiO_2$) are the most used because of their effective UV reflection and transparency [2]. n-$TiO_2$ occurs naturally in three crystalline structures: rutile, anatase, and brookite; rutile is the most common and stable form of this pigment [3]. These particles are utilized in sunscreens since they reflect and absorb UV photons, and their ability to protect against UV exposure is directly related to particle size [4]; n-$TiO_2$ have UVB (290–320 nm) and UVA (320–400 nm) protection; however, the absorption spectrum shifts to a predominantly UVB spectrum as the particle size decreases [5]. The increased use of these products in sunscreens leads to their escalated release to surface waters. For instance, Gondikas et al. depicted an increase of Ti-containing particles, stemming from sunscreens, in the Old Danube Lake (Vienna, Austria), which is heavily used for recreational activities like bathing and water sports during the summer seasons [6]. Similarly, Meyer et al. [7] made a systematic review about ecological impacts of recreational activities in water bodies, concluding that the concentration of UV-filters in lakes generally increases in the summer months. Studies also

indicated the potential risks of using sunscreens in coastal marine areas by tourists, which can inhibit the growth of marine phytoplanktons [8]. The release of n-$TiO_2$ in aqueous environments arises environmental concerns since these particles have been recognized for their light-induced biocidal effects such as negative effects on growing algae as the primary producers in aquatic environments [9,10]. Brunelli et al. [11] observed that in synthetic and real waters, agglomeration and sedimentation depend mostly on the n-$TiO_2$ initial concentrations; hence, a higher bioavailable n-$TiO_2$ fraction in the aquatic environments leads to higher toxic effects [12]; however, the toxicity of n-$TiO_2$ can depend on many other factors including size, surface area, and surface functionalization [13,14].

Once nanoparticles are released to the aqueous environments, they interact with natural organic matter (NOM), which is a complex mixture of organic molecules and a key component in aquatic environments [15,16]. Humic substances, e.g., fulvic acids (FA) [17–20], are important reactive fractions of NOM in soils, sediments, and waters. The exposure of n-$TiO_2$ to humic substances leads to the formation of natural coatings, which impacts the fate of nanoparticles in aqueous environments [21,22]; in other words, adsorption of NOM affects the surface speciation and net charge of the nanoparticles and is therefore of great importance for their colloidal stability, which can alter the mobility and influence the behavior, fate, transport, and bioavailability of the nanoparticles in aquatic environments [23,24]. There is an extensive body of studies about the sorption of NOM onto n-$TiO_2$ using pure n-$TiO_2$ such as P25 [25–31]; for instance, Jayalath et al. [32] investigated the impact of size and pH on the adsorption of humic acids on pure n-$TiO_2$ and concluded that, under their reaction conditions, adsorption is more dependent on the pH than size. However, n-$TiO_2$ used in sunscreens are generally coated with $SiO_2$, $Al_2O_3$, and/or polydimethylsiloxane (PDMS), for instance, in order to tune their properties in the formulation (e.g., PDMS to improve dispersion or $Al_2O_3$ to decrease in photocatalytic activity) [33]. Therefore, recent studies have been conducted on UV-filter starting materials used by the cosmetic industries. For instance, Labille et al. [34] investigated the aging of the $TiO_2$ nanocomposite T-Lite. Similarly, Nickel et al. [35] used $TiO_2$ nanomaterials coated with aluminum oxide and polydimethylsiloxane to investigate their fate and behavior in environmental media. Slomberg et al. assessed the release, fate, and transformation of commercial nanocomposite $TiO_2$ UV filters, with hydrophobic ($Al_2O_3$/stearic acid) and hydrophilic ($SiO_2$) surface coatings in ultrapure water and simulated fresh and seawater [1]. Nonetheless, there is still a lack of studies addressing the effects of n-$TiO_2$ aged in the final product, which is the next step for increasing the environmental relevance of the results.

Characterization of humic substances sorbed onto nanoparticles, i.e., natural coatings, is a challenging step due to the fractionation of humic substances, regarded as supramolecular assemblies of several thousands of different molecules [36,37]. Galindo et al. [38] investigated the molecular level fractionation of a reference fulvic acid (SRFA) during its sorption on an alumina surface using ESI-FTMS (electrospray ionization—Fourier transform mass spectrometry) analysis; they detected ~5700 compounds partitioned between the solution and alumina surface to quite varying degrees, which confirmed the complexity of such systems. On the other hand, the presence of initial coatings on the surface of the n-$TiO_2$ makes these systems more complex. Different surface analytical methods are used to analyze the natural coatings including electron spectroscopies, ion-based methods, scanning probes, etc. [39]. Among these methods, time-of-flight secondary ion mass spectrometry (ToF-SIMS) benefits from high sensitivity to elements and molecules with detection limits in the ppm range [40], ability to detect all isotopes, excellent spatial resolution, applicability on conductive and insulating surfaces, and simultaneous imaging of the surface distribution of detected molecules and elements [41]. For instance, ToF-SIMS is used to analyze the protein adsorbate on gold nanoparticles [41], and $TiO_2$ nanotubes [42]. Stepien et al. investigated the chemical composition of n-$TiO_2$ coated paper surface, declaring ToF-SIMS can yield more detailed insight into surface chemistry compared to X-ray photoelectron spectroscopy [43]. As reviewed in [44], there is an overlap between SIMS and matrix-assisted laser desorption ionization mass spectrometry (MALDI-MS), for obtaining spectra data or

even images [45]. Sophisticated matrix materials, like metallic nanoparticles [46], allowing for very efficient charge and thermal transfer from these matrices to the analytes in the LDI process require thorough mixing of analytes and matrix material and often diffusion of analyte molecules to the matrix nanoparticles. Since a free diffusion of fulvic acids adsorbed on the n-$TiO_2$ to these designed particles acting as the LDI matrix is hindered, the more direct approach based on SIMS was used in this study instead. Similar to LDI data, SIMS data can benefit greatly from the application of high-dimensional data analysis.

Due to the complexity of the abovementioned systems, the classical mass-interpretation methods were replaced with advanced data analysis techniques. For instance, Aoyagi et al. [47] conducted an interlaboratory study on the identification of the peptide sample ToF-SIMS data by machine learning where the spectra of the test peptide sample were predicted by random forest. Also, in medical studies, Zhang et al. [48] used machine learning algorithms on serum blueprints extracted from LDI-MS for the diagnosis of coronary heart disease. In this study, we tried to elucidate the capability of ToF-SIMS supported by high-dimensional data analysis to fill the gap between the sorption of NOM onto model nanoparticles usually used in studies (e.g., P25) and the more complex particles found in commercial products like sunscreens. Hence, we used a mild n-$TiO_2$ extraction method with minimal surface modifications [49]. Moreover, ToF-SIMS, as a surface-sensitive analysis, was used for characterizing the surface of n-$TiO_2$ extracted from ten different sunscreens (n-$TiO_2$ $\subset$ sunscreen), and subsequently, for characterizing the interactions of FA with these particles. Due to the detection of several-hundred masses on each sample, high-dimensional data analysis, namely, cluster analysis and random forest (RF) were used to evaluate the ToF-SIMS data; the former could differentiate between the surface of n-$TiO_2$ $\subset$ sunscreens before and after exposure to FA as well as show a unique sorption pattern for each sample based on the initial sunscreen, and the later could specify explicit masses that are important in sorption. Here, we represent a potential ToF-SIMS combined with high-dimensional data analysis method to study the sorption of fulvic acids onto realistic nanoparticles; therefore, this study can be considered as initial steps for future studies about the interactions of aged nanoparticles (in commercial products) in natural environments.

## 2. Materials and Methods

### *2.1. Sequences of the Study*

Sequences of the study are shown in Figure 1. Part A depicts the effort to find a universal pattern representing the sorption of fulvic acids onto n-$TiO_2$ $\subset$ sunscreen particles, i.e., all the ten sunscreens are evaluated simultaneously where cluster analyses were used for classification. In part B of the study (Figure 1–Part B), each sunscreen was investigated individually where random forest was used to depict the important masses as indicators for sorption of fulvic acids onto each sunscreen. Finally, we aimed at assigning the important masses to the chemical formula to depict which components of fulvic acids are sorbed onto each n-$TiO_2$ $\subset$ sunscreen.

### *2.2. Selected Sunscreens*

Ten commercially available sunscreens (Table S1) were purchased at local shops in Landau in der Pfalz, Germany. The selected sunscreens consist of different sun protection factors (SPFs), textures (lotion or cream), and specificities (dedicated to infants, sensitive skins, or biological, for instance). A detailed list of ingredients can be found elsewhere [49]. All the samples contain $TiO_2$ as the main inorganic component; besides, in some cases, PDMS, $SiO_2$, and $Al_2O_3$ as minor ingredients.

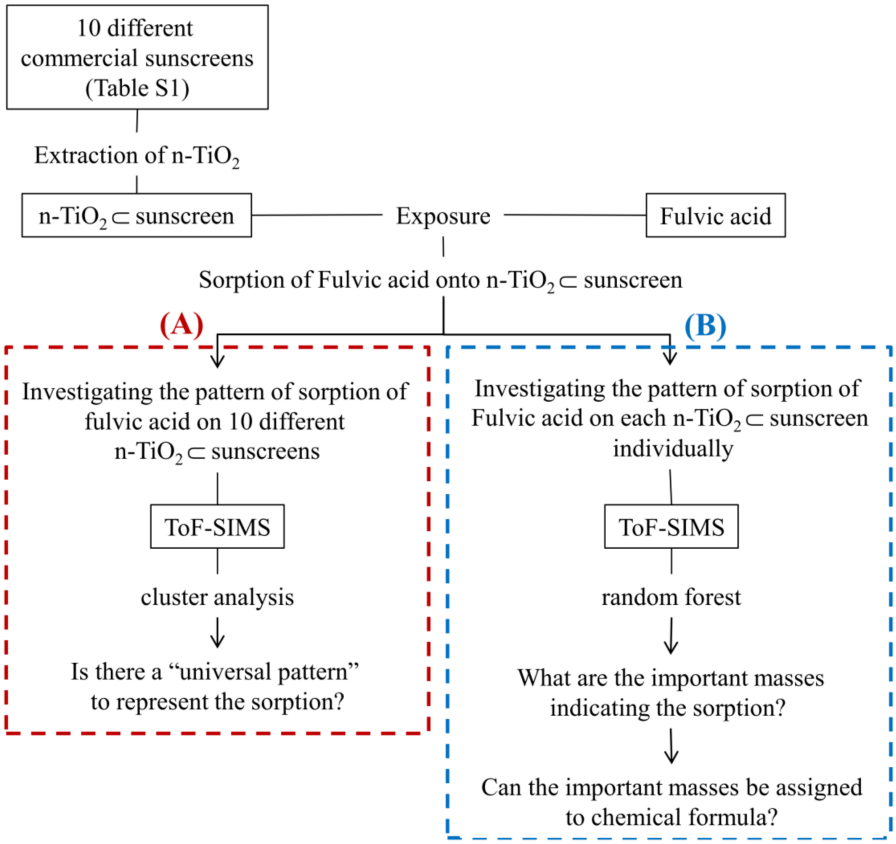


**Figure 1.** The sequence of study of sorption of fulvic acids onto n-$TiO_2$ extracted from sunscreen (n-$TiO_2$ ⊂ sunscreen).

### *2.3. Extraction of $TiO_2$ Nanoparticles from Sunscreens*

Extraction of $TiO_2$ from each sunscreen was performed following Philippe et al. [49]. Extraction of sunscreens 1–7 in Table S1 (were completely dispersible in 0.1% Triton X-100): Sunscreen bottles were vigorously shaken before opening. A total of 50 mg of each sunscreen and 10 mL of 0.1% Triton X-100 (Alfa Aesar, Kandel, Germany) aqueous solution with a pH adjusted to 12 with NaOH (p.a., Sigma-Aldrich, Taufkirchen, Germany) was stirred in a glass beaker for 30 min until a homogeneous suspension was obtained. They were transferred to ultrafiltration units (Amicon Ultra-15 Centrifugal Filter Tubes, Millipore, Merck, Darmstadt, Germany; cut-off: 30 kDa) and centrifuged at 4500 r.p.m. for 30 min using a Universal 320 centrifuge from Hettich Zentrifugen (Tuttlingen, Germany). The filtrates from the tube were discarded and the concentrates were redispersed in 10 mL of the Triton X-100 solution. In total, the filtration and resuspension (in surfactant) steps were repeated three times. Consequently, the samples were also rinsed three times using demineralized water by ultrafiltration. Extraction of sunscreens 8–10 in Table S1 (were not completely dispersible in 0.1% Triton X-100): Sunscreen bottles were vigorously shaken before opening. 50 mg of each sunscreen was suspended in n-hexane (Rotisolv HPLC, Carl Roth, Karlsruhe, Germany) and then centrifuged in glass tubes at 5000 r.p.m. for 20 min. Consequently, the centrifugates were redispersed in a 0.1% Triton X-100 and the same procedure (as for sunscreen 1–7) was carried on them. The final extracted samples were dispersed in 10 mL demineralized water (to avoid drying) and kept in the dark at 4 °C. The recovery (%), shape, size, and isoelectric point of the extracted $TiO_2$ nanoparticles for each sunscreen are reported elsewhere [49].

### *2.4. Preparation Suwannee River Fulvic Acids (FA) Stock Solution*

Suwannee River Fulvic Acids (SRFA) standard II was purchased from the International Humic Substances Society (IHSS, St. Paul, MN, USA). The elemental compositions of this sample provided by the supplier can be found in Table 1.

**Table 1.** The elemental compositions in %(*w*/*w*) of SRFA provided by IHSS.

| | $H_2O$ [1] | Ash [2] | C [3] | H [3] | O [3] | N [3] | S [3] | P [3] |
|---|---|---|---|---|---|---|---|---|
| Standard FA II | 16.9 | 0.58 | 52.34 | 4.36 | 42.98 | 0.67 | 0.46 | 0.004 |

[1] in the air-equilibrated sample (a function of relative humidity). [2] inorganic residue in a dry sample. [3] elemental composition of a dry, ash-free sample.

The stock solution of FA was prepared according to Metreveli et al. [50]. A total of 10 mg FA was dissolved in 50 mL demineralized water. The pH was adjusted to 10 using NaOH (p.a., Sigma-Aldrich, Taufkirchen, Germany). The solution was filtered using a 0.1µm cellulose nitrate membrane filter (Whatman, Dassel, Germany) to remove undissolved fractions and stirred with a magnetic stirrer for 24 h. The prepared FA stock solution was stored in the dark at 4 °C. The fresh 10 mg/L of FA solution was being prepared before each exposure experiment.

### 2.5. Exposure of $TiO_2$ Nanoparticles Extracted from Sunscreen to Fulvic Acids

The suspension of n-$TiO_2$ extracted from 50 mg of sunscreens (the final content of n-$TiO_2$ extracted from 50 mg of each sunscreen is shown in Table S1) was ultrasonicated for 10 min and 40 mL of the FA solution (10 mg/L) was added. The samples were shaken at 200 r.p.m. using a horizontal shaker at room temperature (21 °C) for four days. Afterward, the suspensions were centrifuged (4500 r.p.m. for 30 min), the supernatant was removed and the particles were rinsed with demineralized water and centrifuged to remove unattached molecules. They were then resuspended in 10 mL demineralized water prior to shipping for analysis.

### 2.6. ATR-FTIR (Attenuated Total Reflectance—Fourier Transform Infrared Spectroscopy)

ATR-FTIR measurements were carried out according to Tayyebi et al. [28]. Extracted n-$TiO_2$ from sunscreen (4), before and after exposure to fulvic acids, were centrifuged at 4500 r.p.m. (3300 g) for 30 min and freeze-dried (Christ, Osterode, Germany) for two continuous days at −40 °C and 0.12 mbar and two more days at −60 °C and 0.011 mbar. Consequently, about one milligram of the sample was placed directly on the ATR-crystal of an Agilent Cary 630 FTIR spectrometer with a one-reflection diamond ATR element. Spectra were measured against an air background before each sample. The spectral resolution was 4 $cm^{-1}$ and 32 scans were recorded for each spectral measurement (range: 4000–650 $cm^{-1}$). The results were graphed with R (Version R-4.1.0). The presence or absence of ATR-FTIR bands was investigated based on the visual evaluation.

### 2.7. Three-Dimensional Excitation-Emission-Matrix (EEM) Fluorescence Spectroscopy

A total of 1 mg of the freeze-dried samples (mentioned in ATR-FTIR) was suspended in 5 mL deionized water and their fluorescence spectra were recorded on a PerkinElmer LS 55 fluorescence spectrometer in the emission range of 300–700 nm by varying the excitation (Ex) wavelength from 260 to 350 nm in 10 nm increments with a scan rate of 1200 nm $min^{-1}$. No corrections for scattering effects were applied to the data as there was no observable overlapping of the area of interest of fluorescence and scattering peaks. The EEM spectra were plotted using Origin (version 7.5).

### 2.8. Time-of-Flight Secondary Ion Mass Spectrometry (ToF-SIMS)

Upon receiving the suspensions, the particles were further concentrated down to a volume of 100 µL by centrifugation (5000 r.p.m. for 30 min). To obtain a fairly uniform lateral deposition of the particles, the substrates used for SIMS analysis (lapped silicon wafers) were treated thoroughly with UV/ozone (15 min in Ossila UV Ozone Cleaner 2.0, Ossilia BV, Leiden, The Netherlands) prior to distributing the sample suspensions onto them. The sample was placed in a spin coater (model WS-650MZ-23, Laurell Technologies Corporation, North Wales, PA, USA) and the rotation speed was increased gradually up to 100 r.p.m. to allow for a homogeneous distribution and slow drying of the particle

suspensions. The extracted $TiO_2$ nanoparticles from each sunscreen before and after exposure to fulvic acid were analyzed using ToF-SIMS. In addition, a procedural blank (0.1% Triton X-100 in ultrafiltration units without sunscreen) and fulvic acids (10 mg/L) were measured to have a negative and positive control, respectively.

SIMS data were acquired on a ToF5 spectrometer (IONTOF, Münster, Germany) using $Bi^{3+,}$ 25 keV primary ions. Individual fields of view of 500 × 500 $\mu m^2$ were recorded (128 × 128 pixels, total dose density: $1.5 \times 10^{11}$ $cm^{-2}$, static limit).

For part A of our study, 10 individual spots (replicates) from each sample were analyzed in negative secondary ion polarity (as it was expected that due to the presence of many oxygen atoms in FA mostly negatively charged characteristic secondary ions are to be observed). Spectra were mass calibrated on the signals of $C^-$, $CH^-$, $C_2^-$, and $C_3^-$ (usually with mass deviations $\Delta m/m$ in the range < 10 ppm). Using the software Surfacelab 7 (IONTOF, version 7.2.129059) a mass interval list was built holding 198 intervals in the mass spectrum range from 12 m/z (assigned to $C^-$) to 199 m/z (not assigned). This peak picking was performed on the derivative of the smoothened counts versus flight-time spectrum. This approach uses spectral features for guidance, rather than just predefined mass ranges, and can pick several signals on one nominal mass. One example in the low mass range is picking both $^{13}CN^-$ and $C_2H_3^-$, with peaks centered at 27.01 and 27.03 m/z, respectively.

While the instrument is able to deliver good mass resolutions applying a bunched primary ion pulse and a non-linear time-of-flight analyzer (values of >7000 $m/\Delta m$ are reported) the complex nature of the samples of this study limited the mass resolution to approx. 3000–4000 $m/\Delta m$. This is an important constraint hampering the chemical assignment for high mass signals.

For part B of this study, a corresponding analytical approach was used: ToF-SIMS was performed on three individual n-$TiO_2$ ⊂ sunscreen samples (samples 3, 4, and 9) with 72 individual measurements (36 negative polarity replicates measured first, followed by 36 positive polarity replicates measured again from the very same spots) on each sample. Each of these individual fields of view was separated by 100 µm from the adjacent ones in the 6 × 6 array. However, due to the use of freshly prepared samples having a thicker deposition of the $TiO_2$ particles, fewer substrate signals were recorded, but a charge compensation during the measurements was applied (21 eV electron flood gun and tuning the reflectron accordingly). While this keeps the primary ion dose again below the static limit, possible beam damage caused by the electron flood gun did accumulate as we move along the 6 × 6 array since this gun is not focused. Positive polarity spectra were calibrated on $CH_2^+$, $CH_3^+$, $C_2H_2^+$, and $C_5H_7^+$. For data evaluation, peak sets of both polarities were combined.

### *2.9. Data Evaluation*

Cluster analysis was carried out to visualize groups in the global sample pool and subsequently determine if samples with FA were classified differently from samples without FA. Cluster analysis is an unsupervised statistical technique, i.e., no prior specification of groups is required and the similarities of the groups are defined by distances between samples using the Euclidean distance measure. Here, the distances between each sample were calculated based on their SIMS peak intensities and were clustered using divisive hierarchical clustering and K-means clustering. Divisive hierarchical clustering groups similar data together so that similar ones are found in close proximity to each other [51]. Hence, samples with similar secondary ion intensities will be grouped by the clustering algorithms enabling the differentiation between nanoparticles before and after exposure to FA in case their secondary ion spectra differed. Furthermore, through cluster analysis, we might detect general patterns/structures in the mass spectra of the samples. To confirm the results of divisive hierarchical clustering, K-mean clustering, the recommended clustering for big data sets, was also carried out [52]. The optimal number of clusters for k-mean clustering was derived by reallocating samples until the mean silhouette width, i.e., mean similarity for each sample to other objects in its cluster compared to its similarity to the most similar cluster, of each sample, was maximized. Optimal numbers of clusters were

used here since the small number of the clusters might not be able to capture a small but important difference between the groups and the big number of the clusters could make it hard to interpret the character of each cluster [53].

Random forest (RF) models were fitted to distinguish samples with FA and without FA and the variable importance was estimated from RF models using the impurity importance [54]. For the RF model, we used the secondary ion signals (masses) whose intensities increased after exposure to fulvic acids although many signals were decreasing after exposure due to the rinsing effect of the pristine coating. These decreasing signals could potentially be a good predictor for the exposure step from the RF point of view; however, since they are not useful to characterize the FA sorption layer, only the increased-intensity signals were used to identify FA-related new signals on the FX samples. It is also worth mentioning that the increased-intensity masses can be either due to sorbed FA or even can be influenced by the rinsing effect. The latter can be explained by removing the topmost surface layer of the nanoparticles during rinsing; hence, the particle cores underneath can become exposed yielding increased ToF-SIMS signals. To simplify the results, all the increased signals pertained to sorbed FA.

To identify the increased-intensity masses, the intensities of the selected SI peaks recorded from pristine nanoparticles were subtracted from the exposed nanoparticles to fulvic acids, i.e., FX-X. To avoid the effect of small changes on calculations, only significant changes (*t*-test 95% confidence) were used for further evaluations. FX-X > 0 was considered as increased-intensity masses. Consequently, we trained a random forest (RF) model [54], in classification mode with masses of the samples as predictors and a binary response variable indicating if a sample contained fulvic acids or not.

RF algorithms have been proven to perform very well to identify the most important parameters in a data set with a high number of variables compared to the number of observations [54]; they have been applied in different areas successfully, including chemoinformatics [55]. After model training, we identified the most important masses for the differentiation if a sample contained FA or not with the impurity importance from the random forest model [56]. The models' performances evaluated on the test set were satisfying for all masses as reflected in very high accuracies (100%) of the models (Table S2). All data and R-codes are available for download on GitHub (see the "Data Availability Statement" below).

## 3. Results and Discussions

The stepwise procedure to study the sorption of fulvic acids onto n-$TiO_2$ ⊂ sunscreen is shown in Figure 1. It is worth mentioning that samples were initially analyzed using ATR-FTIR. However, no new IR band could be observed on n-$TiO_2$ ⊂ sunscreen after exposure to fulvic acids (Figure S1a). Therefore, ATR-FTIR is not sensitive enough to detect the sorbed components of fulvic acids under those conditions. Three-dimensional excitation-emission-matrix (EEM) fluorescence spectroscopy could not either detect any fluorophore fraction of fulvic acids (excitation/emission ~ 310/450 nm) [57] being sorbed onto nanoparticles (Figure S1b). Hence, only the results from ToF-SIMS are discussed further.

Figure 1—Part (A) shows our approach of finding a universal pattern to represent the sorption of fulvic acids onto n-$TiO_2$ ⊂ sunscreen (10 sunscreens, 9 replicates each); Part (B) limits down the number of samples and studies them individually in detail (36 replicates each), i.e., searching for specific masses, which represent sorption of fulvic acids on each n-$TiO_2$ ⊂ sunscreen.

### *3.1. Part (A): Searching for a Universal Pattern to Represent the Sorption of Fulvic Acids onto Sunscreens' Nanoparticles*

Extracted $TiO_2$ nanoparticles from ten different sunscreens were analyzed before and after exposure to fulvic acids using ToF-SIMS. The divisive hierarchical clustering analysis of the obtained masses revealed, as expected, that it is possible to differentiate between X and FX where X and FX are grouped differently in divisive hierarchical clustering (Figure 2). For

instance, samples 1 and F1, also 3 and F3, and 7 and F7 were completely separated. Similarly, the sub-clusters of exposed and non-exposed are readily observed for 4 and F4, 5 and F5, 6 and F6, 8 and F8, and 9 and F9 (an exception is seen for 2 and F2 that are mixed in a branch implying they are indistinguishable from each other). Hence, although ToF-SIMS results do not show a universal FA adsorption pattern on the n-$TiO_2$ ⊂ sunscreens, they can be potentially used to identify the origin of each n-$TiO_2$ since the fragment patterns differ for each sunscreen, which shows changes on the surface coating are detectable by ToF-SIMS.

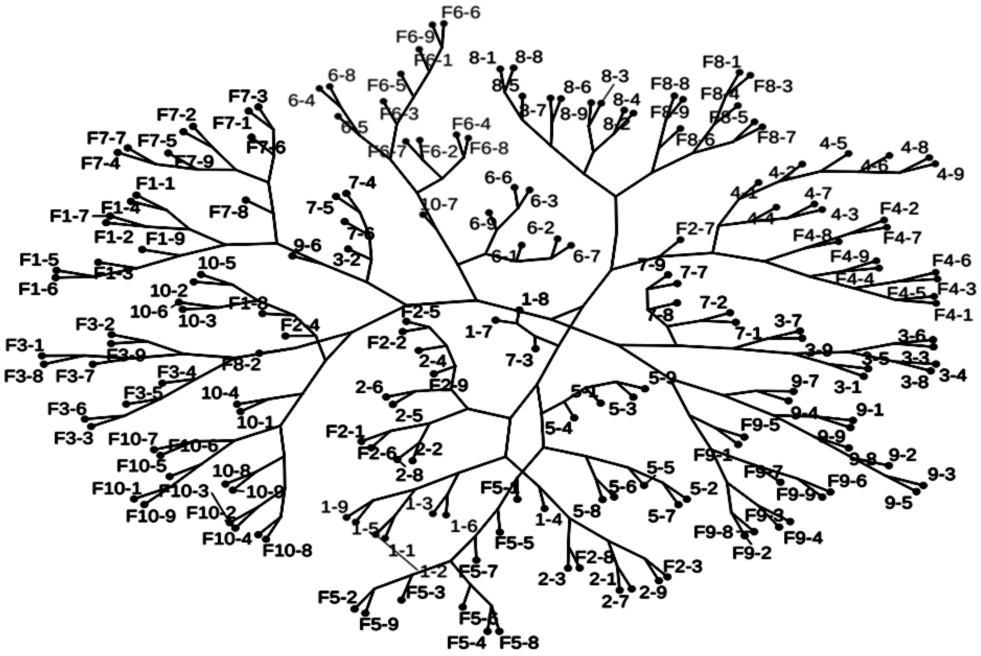


**Figure 2.** Visualization of the divisive hierarchical clustering of n-$TiO_2$ ⊂ sunscreen samples from 10 different sunscreens before (X-Y) and after (FX-Y) exposure to fulvic acids where X and Y depict the number of each sunscreen and the number of replicates measured by ToF-SIMS, respectively. F represents the exposure to fulvic acids.

Furthermore, the patterns of FX differ for each sample (Figure 2). For instance, F1, F3, F4, etc. are grouped differently, i.e., the surface of n-$TiO_2$ ⊂ sunscreens are not streamlined in the presence of fulvic acids. This phenomenon may have two reasons; either exposure to fulvic acids does not result in a detectable change on the surface of nanoparticles or the initial differences on the surface of each n-$TiO_2$ ⊂ sunscreen result in different sorbates' structures. Considering that the lengths of the paths between the nodes (Figure 2) represent proximities between the objects, [58], the closer the sub-groups in divisive hierarchical clustering, the more similarity of the surface chemistry of the nanoparticles can be expected. Interestingly, although some X and FX samples are grouped close to each other, e.g., 9 and F9, other samples bear a big distance, e.g., 3 and F3. This phenomenon shows that n-$TiO_2$ extracted from different sunscreens behave differently getting exposed to fulvic acids. In some cases, their surface compositions still contain enough information to be traced back to the original coating, while in some others the n-$TiO_2$ ⊂ sunscreens cannot be identified after exposure. In other words, the found mass patterns on the surface of n-$TiO_2$ ⊂ sunscreens exposed to fulvic acids are samples-specific. K-mean clustering (Figure S2) confirms the separation of FX-Y and X-Y similar to divisive hierarchical clustering. Moreover, each exposed sample is grouped in a different cluster (e.g., F8 is grouped differently from F4), which depicts the unique pattern of sorption on each sunscreen.

In order to understand the nature of the differences between n-$TiO_2$ ⊂ sunscreen before and after exposure to fulvic, significant (t-test 95%) differences in the intensities of all detected fragments between the means of nine replicates before and after exposure were determined (Figure S3**)**. All n-$TiO_2$ ⊂ sunscreen samples had at least a couple of

masses whose intensities increased after exposure to fulvic acids, except sample 2. Sample 2 showed no difference on the surface after exposure to fulvic acids; it is in agreement with the divisive hierarchical clustering (Figure 2), in which 2 and F2 were not grouped separately probably due to a lack of sorption on these particles; hence, this sample was not used for further interpretations.

Masses with an increase in their intensities after exposure to fulvic acids (FX-X > 0) can indicate the sorption of molecules with different compositions compared to the genuine coating. The increased-intensity mass patterns (based on mass intensity) differ strongly from one sample to the other (Figure S3), indicating that different components of fulvic acids are sorbed on the surface of each n-$TiO_2$ ⊂ sunscreen. Table S3 summarizes the number of masses whose intensities increased after the exposure process. So, each n-$TiO_2$ ⊂ sunscreen exposed to fulvic acids can be compared pairwise to other samples to evaluate if there are masses whose intensity increased after exposure, which are common to two or more sunscreens' nanoparticles. The strongest overlap was found for n-$TiO_2$ ⊂ sunscreen 4 and 9 exposed to fulvic acids with 17 common increased masses. The other samples have few common increased masses, e.g., samples 1 and 3 have one, or samples 4 and 7 show no common increased mass after exposure to fulvic acids. Subsequently, there is no common peak that increased for all the samples, which implies different fractionation of fulvic acids on each n-$TiO_2$ ⊂ sunscreen. Here, we just considered the increased-mass intensities (FX-X > 0) as a conservative sign for sorption. However, there are also masses whose intensities decreased after exposure of n-$TiO_2$ ⊂ sunscreen to fulvic acid (FX-X < 0); the reason for decreased-intensity mass after exposure to fulvic acids is discussed in part B.

In summary, we found no universal pattern to represent the sorption of fulvic acids onto different n-$TiO_2$ ⊂ sunscreens. Although the exposure has affected the surface coating to the extent that the differentiation between FX and X is possible for almost all the sunscreen extracts (Figure 2), there are no similar sorption patterns among different FXs. In other words, exposure to fulvic acids significantly affects the surface coating of n-$TiO_2$ ⊂ sunscreen; however, it is not enough to erase the specificity on each original coating. Hence, under the reaction conditions, the specifications of n-$TiO_2$ in sunscreens (variables such as size, shape, isoelectric point, coating, and n-$TiO_2$ content) affect the sorption. It has to be noted that several potentially relevant characteristics such as the level coating coverage, the thickness of the coating, for instance, were not available. Therefore, a discussion about how nanoparticle characteristic triggers the composition of the sorption layer is beyond the aim of this paper. However, our results suggest a complex interplay between these characteristics.

### *3.2. Part (B): Investigating the Sorption's Pattern on each Sunscreen Individually*

#### 3.2.1. Important Masses Indicating the Sorption

Part A suggests that there are indicator masses for each sunscreen characteristic for the sorption of fulvic acids, which could be used as predictors. To improve the prediction of each sunscreen, ToF-SIMS was performed on the n-$TiO_2$ ⊂ sunscreen samples 3, 4, and 9, which had a thicker deposition of particles on the carriers. The samples were chosen based on their initial surface coatings [49]; where 3 and 4 have PDMS (polydimethylsiloxane) and 9 has Aluminum oxide coating. Similar to part A (Figure 2), the selected three sunscreens, with a higher number of replicates (36 per polarity), depicted a unique feature for each extracted nanoparticle after exposure to fulvic acids (Figure S4). K-Mean clustering (Figure S5) is also in agreement with divisive hierarchical clustering, which differentiates the n-$TiO_2$ ⊂ sunscreen before and after exposure to fulvic acids. Interestingly, K-mean clustering shows a difference on the surface of the same n-$TiO_2$ ⊂ sunscreen; for instance, sample 9 is grouped into two clusters roughly following the replicates' IDs. This is due to the fact that here a low energy electron beam was used for charge compensation on a thicker deposition of particles on the carriers (for measuring a high number of replicates), thereafter, we observed, especially in the high mass range, some electron beam effects, usually leading to decreasing intensities from unstable fragments. This observation is in accordance with the findings of R. Havelund

et al. [59]. Since all samples were analyzed following strictly the same protocol we refrained from any attempts to correct data with mathematical post-processing.

In the next step, the nature of the changes of n-$TiO_2$ ⊂ sunscreen after exposure to fulvic acids was investigated. Figure 3 shows the normalized intensity mean difference between each sample pair before and after exposure to fulvic acids, i.e., FX-X. All samples show increased intensities (FX-X > 0) for both negative and positive polarities, which indicate the sorption of fulvic acids on the surface of particles. Apart from increased-intensity masses, there are also decreased-intensity masses (FX-X < 0), i.e., some sunscreen components, which remained attached to the n-$TO_2$ surface desorbed during exposure to fulvic acid. This desorption may also be promoted by the sorption of fulvic acids in a ligand exchange process. To clarify this point, n-$TiO_2$ ⊂ sunscreen (3) was exposed to MQ water (without fulvic acids) and the obtained ToF-SIMS results were compared to initial n-$TiO_2$ ⊂ sunscreen (3) (Figure S6). The comparison, i.e., 3 (MQ water-exposed)-3, clearly shows that many molecules from the coating are desorbing during exposure to pure water. Hence, we can assume that most of the decreased-intensity masses correspond to components from desorbed molecules. There are also some increased-intensity masses after rinsing with MQ water; as described in data evaluation, this phenomenon is due to exposing components from the cores of the n-$TiO_2$ particles detected by ToF-SIMS. To increase the focus on characterizing the fulvic acids coating, only the masses whose intensities increased after the FA exposure were used for further evaluations with RF.

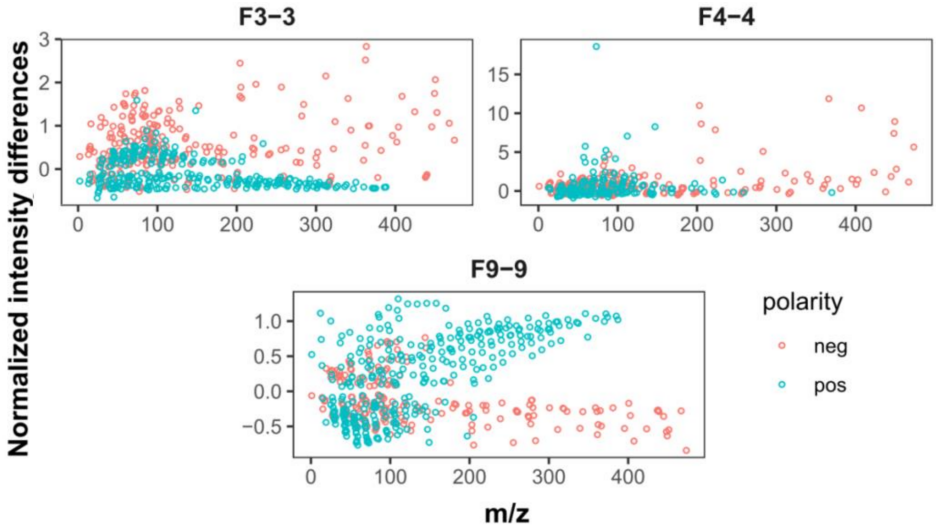


**Figure 3.** Differences in the mean of normalized intensities for exposed (FX) and non-exposed (X) samples to fulvic acids (FX-X: F3-3, F4-4, and F9-9) averaged over 36 replicates. Red dots depict negatively charged ions, and blue dots depict positively charged ions measured by ToF-SIMS.

The results of the variable importance obtained from RF analysis, i.e., the most important signals for predicting the sorption of fulvic acids onto samples 3, 4, and 9, clearly showed that each n-$TiO_2$ ⊂ sunscreen sample has a unique set of important masses after exposure to fulvic acids (Figure 4). For instance, the five most important masses for sunscreen 3 (Figure 4a) are neg13.008, neg32.9, neg280.84, neg110.02, and neg79.961 m/z, while for sunscreen 4 (Figure 4b) these are neg84.975, neg39.974, neg51.975, neg13.008, and neg100.971 m/z ("neg" indicates negatively charged secondary ions). For sample 9 (Figure 4c), the five most important masses are positively charged fragments, i.e., pos253.058, pos151.03, pos164.036, pos300.04, and pos301.043; in agreement with Figure 3 showing that most of the increased-intensity signals for sample 9 after exposure to fulvic acids (F9-9 > 0) are positively charged ions. The variety of important masses evaluated using RF confirms the aforementioned discussion in part (A), which demonstrates the dependency of sorption on the initial composition of each sunscreen. Also, as it was mentioned in part (A), although samples 3 and 4 had the same initial PDMS coating (Table S1),

they showed different important masses in RF, which implies that the original coating is not the only influential variable in sorption, while multi variables (size, shape, isoelectric point, coating, etc.) can trigger the fractionation of fulvic acids being sorbed onto nanoparticles.

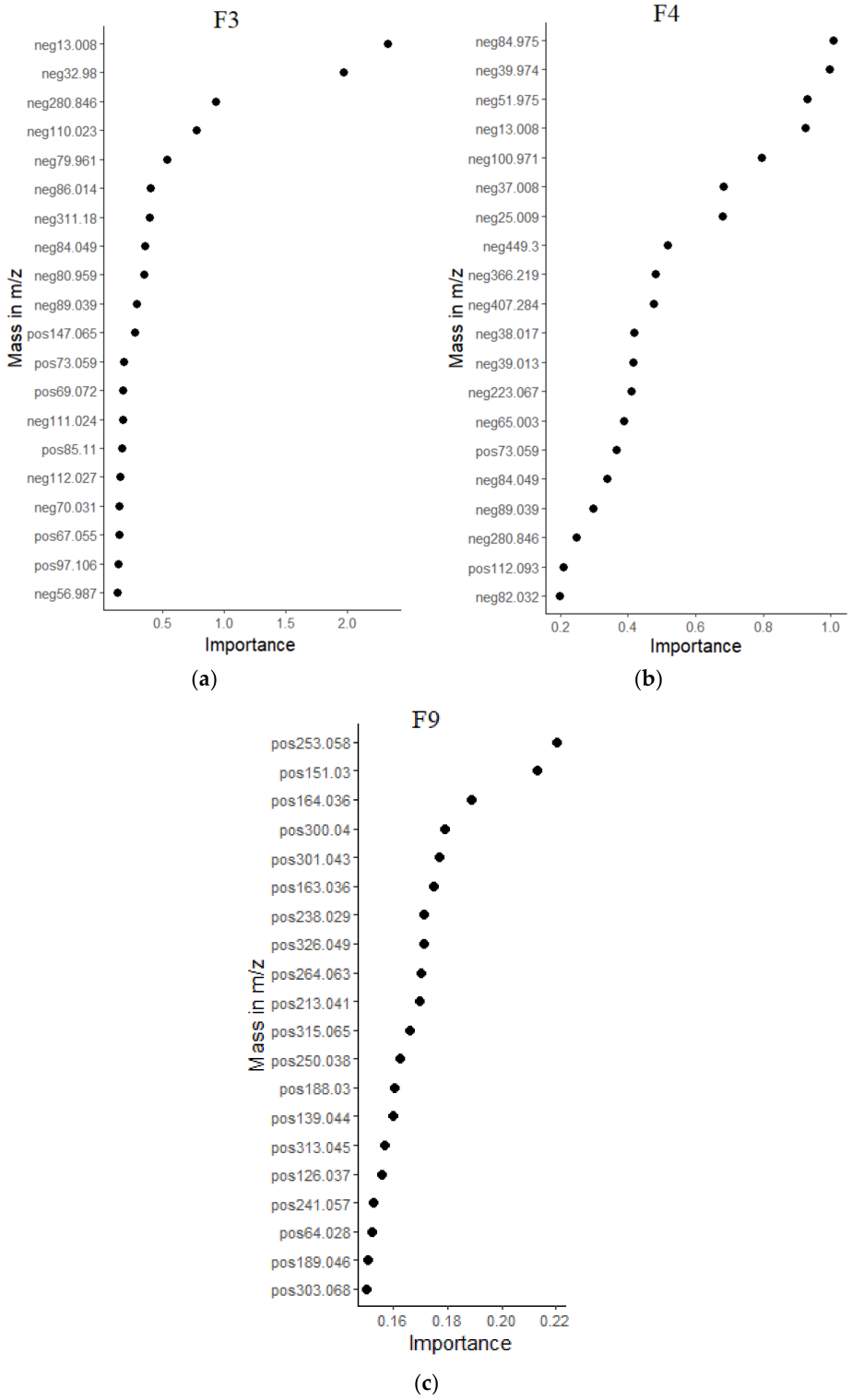


**Figure 4.** The pattern of impurity-based important masses depicting sorption of fulvic acids onto n-$TiO_2$ ⊂ sunscreen evaluated by using RF. (**a**) n-$TiO_2$ ⊂ sunscreen (3) exposed to fulvic acids; (**b**) n-$TiO_2$ ⊂ sunscreen (4) exposed to fulvic acids; (**c**) n-$TiO_2$ ⊂ sunscreen (9) exposed to fulvic acids ("neg" and "pos" indicates negatively and positively charged secondary ions).

3.2.2. Possible Molecular Structures

We attempted to link the important masses, obtained using RF, to possible molecular structures (stoichiometries) of the sorbed components of fulvic acids; hence as an example, the most important masses related to the sorption of fulvic acid onto n-$TiO_2$ ⊂ sunscreen (3) were chosen for further investigations (Figure 4a).

In general, the lower the masses (m/z), the easier they can be assigned to chemical moieties. For F3, the most important mass, i.e., neg13.008 m/z, can be unambiguously assigned to $CH^-$ (Figure S7—up), which is an unspecific marker for organic coatings [60]. However, considering the complexities of the studied samples, especially FA being a mixture of many different compounds with only partially known chemistries, and the limited mass resolutions obtained in the analyses, the higher masses cannot be attributed to a unique fragment. To overcome this drawback, we used the correlation matrix among increased masses (Figure S8) combined with a priori knowledge about potential structural links between the fragments to connect large fragments with small and easily identified ones, hence, enabling us to select the most plausible sum formula. For instance, the second and fifth important masses, i.e., neg32.9 and neg79.961 m/z, are positively correlated (R > 0.7); and both contain sulfur since their assignments are $SH^-$, and $SO_3{}^-$, respectively (Figure S7—down). It is also in agreement with the presence of S in the structure of FA (Table 1) that can be the source of sulfur-containing components in n-$TiO_2$ ⊂ sunscreen(3) exposed to fulvic acids. In principle, for sulfur, also the characteristic isotopic distribution (95% $^{32}S$ and 4% $^{34}S$) could be used to verify these assignments, but in this study signals for $^{32}SH^-$ signals were weak, and $^{34}SH^-$ overlapped with the much stronger signal of $^{35}Cl^-$. Signal neg280.84 as the third important mass belongs to a very weak and poorly mass resolved signal from the F3 sample; the average intensity of this peak in the F3 set was 265 ± 62 counts as compared to 137 ± 35 counts in the untreated samples (average noise level is 50 counts). Therefore, it cannot be assigned to any fragments. Mass neg110.023 is the fourth important signal and correlates only weakly (correlation coefficient < 0.4) with the aforementioned signals of neg32.98 ($SH^-$) or neg79.961 ($SO_3{}^-$); hence, sulfur components can be ruled out in this case. Nonetheless, there are high correlations (correlation coefficient > 0.6) between the neg110.023 signals and the signals neg85.015, neg86.014, neg13.008 ($CH^-$), neg25.009 ($C_2H^-$), neg37.008 ($C_3H^-$), neg111.023, and neg112.027 (Figure S8).

These correlated peaks are spaced by 1 amu on the mass scale (Table 2), meaning that they reflect partially the $^{13}C$ isotope pattern as well as hydrogen addition/abstraction products, which is further confirmed by the presence of low molecular weight hydrocarbons. Furthermore, the correlation to the 85–86 range (neg85.015 and neg86.014) is remarkable; this is due to the abstraction of $C_2H$ from the parent fragment at 110 m/z. Hence, neg110.023 is probably composed of hydrocarbon moieties.

**Table 2.** Signal intensities of highly correlated unassigned peaks from n-$TiO_2$ ⊂ sunscreen (3).

| | **Mean Intensity ± Standard Deviation for Set F3 [$10^3$ cts]** | **Mean Intensity ± Standard Deviation for Set 3 [$10^3$ cts]** |
|---|---|---|
| Neg85.015 | 5.5 ± 1.3 | 5.1 ± 0.8 |
| Neg86.014 | 3.5 ± 0.8 | 3.2 ± 0.4 |
| Neg110.023 | 2.7 ± 0.5 | 2.0 ± 0.2 |
| Neg111.023 | 2.0 ± 0.7 | 1.1 ± 0.3 |
| Neg112.027 | 1.4 ± 0.4 | 0.8 ± 0.2 |

In summary, RF is a powerful tool for finding out the important masses indicating the sorption of fulvic acid on each n-$TiO_2$ ⊂ sunscreen. The important masses represent the pattern of sorption and can be used to distinguish between the nanoparticles before and after exposure to fulvic acids. The attempts to assign the important masses to the chemical fragments showed that some of the lower masses (<100 amu) can be assigned to chemical fragments, either directly or by using a correlation map, the high masses (>100 amu) cannot

be precisely assigned due to the complexity of the reaction matrix and the possibility of the existence of multiple fragments for each mass to the corresponding charge ratio (m/z).

## 4. Conclusions

This work represents the first steps towards a more complete characterization of natural coatings formed onto nanoparticles. We showed here that ToF-SIMS provides enough information to detect natural coatings and to account for small differences between sunscreen samples. However, using ToF-SIMS ends with a large number of variables (masses) and replicates requiring statistical methods for data evaluation. Hence, a machine learning method, i.e., RF was used as a tool to find the most important masses that indicate sorption. The results demonstrate that the extracted $TiO_2$ nanoparticles of each sunscreen react differently with fulvic acids, which are composed of a mixture of several compounds. In other words, the original specifications of the nanoparticles in each sunscreen (e.g., size, original coating, etc.) are the factors controlling the fractionation of fulvic acids in sorption. Therefore, under the reaction conditions, we could not find a universal pattern for the sorption of fulvic acids onto n-$TiO_2$ ⊂ sunscreens. Moreover, since the differences in sorption of fulvic acids can affect the aggregation, deposition, and reactivity of the nanoparticles, which subsequently lead to differences in fate, the studied samples, with different sorption patterns, can differ in terms of fate.

Future work should focus on the development of the characterization of natural coatings, e.g., analysis of different types of NOM (humic substances, polysaccharides, and proteins) including their combinations under environmentally relevant conditions, and improving the tools to find some formula accounting for correlations, etc. Moreover, the assignment of mass markers to chemical fragments is important to know the mechanisms of the formation of natural coatings. A possible way forward could be to combine ToF-SIMS with other techniques (2D-correlation) to identify the fragments.

**Supplementary Materials:** The following are available online at https://www.mdpi.com/article/10.3390/coatings12030335/s1, Sorption of fulvic acids onto titanium dioxide nanoparticles extracted from commercial sunscreens: ToF-SIMS and high-dimensional data analysis, Table S1: ID numbers, SPF, and the used inorganic particles ($TiO_2$, $SiO_2$, and $Al_2O_3$) of the 10 studied sunscreens based on the information written on their packages. Table S2: Summary of random forest models performances. Figure S1a: Representative ATR-FTIR spectra of the n-$TiO_2$ ⊂ sunscreen(4) before and after exposure to fulvic acid. Figure S1b: Three-dimensional excitation-emission-matrix (EEM) fluorescence spectroscopy of n-$TiO_2$ ⊂ sunscreen(4) exposed to fulvic acid. No peaks depicting the presence of fulvic acids (excitation/emission ~ 310/450 nm) can be detected on the nanoparticles (The color scale depicts the intensity, and the black lines depict Raman and Rayleigh scatterings). Figure S2: K-mean clustering of n-$TiO_2$ ⊂ sunscreen samples for 10 different sunscreens before (X-Y) and after (FX-Y) exposure to fulvic acid. Figure S3: Differences in the normalized intensities (negative polarity) averaged over 9 replicates for all masses detected using ToF-SIMS for n-$TiO_2$ ⊂ sunscreen samples before and after exposure to fulvic acids. Table S3: The number of common masses of n-$TiO_2$ ⊂ sunscreen samples with increased-signal intensities after exposure to fulvic acids. Figure S4: The number of common masses of n-$TiO_2$ ⊂ sunscreen samples with increased-signal intensities after exposure to fulvic acids. Figure S5: K-mean clustering of n-$TiO_2$ ⊂ sunscreen (samples 3, 4, and 9) before (X-Y) and after (FX-Y) exposure to fulvic acid. Figure S6: The intensity difference between 3 (MQ water-exposed)-3 where 3 (MQ water-exposed) is n-$TiO_2$ ⊂ sunscreen (3) exposed to pure water (instead of fulvic acid), and 3 depicts the initial n-$TiO_2$ ⊂ sunscreen (3). Figure S7: Mass neg13.008, neg32.98, and neg79.961, on the surface of n-$TiO_2$ ⊂ sunscreen(3) exposed to fulvic acid, assigned to $CH^-$, $SH^-$, and $SO_3{}^-$, respectively. Figure S8: The correlation matrix of increased masses for sample F3 i.e., n-$TiO_2$ ⊂ sunscreen(3) exposed to fulvic acids.

**Author Contributions:** Conceptualization, N.T.S.K. and A.P.; Methodology, A.P. and N.T.S.K.; Software, A.P.; Validation, N.T.S.K. and A.P.; Formal analysis, A.P. and S.K.; Investigation, N.T.S.K. and A.W.; Data curation, A.W. and A.P.; Writing—original draft preparation, N.T.S.K.; Writing—review and editing, S.K., A.W., A.P. and N.T.S.K.; Visualization, S.K. and A.P.; Supervision, A.P.; Project administration, A.P. All authors have read and agreed to the published version of the manuscript.

**Funding:** This research was funded by the German Research Foundation, research unit INTERNANO (FOR1536 "Mobility, aging and functioning of engineered inorganic nanoparticles at the aquatic-terrestrial interface", subprojects SCHA849/16). The publication was funded by the Open Access Fund of the University of Koblenz-Landau.

**Institutional Review Board Statement:** Not applicable.

**Informed Consent Statement:** Not applicable.

**Data Availability Statement:** The data evaluations were performed using R (Version R-4.1.0). The complete R-code and the ToF-SIMS raw data are available on: https://github.com/KunzstLD/Nanoparticle_classification (accessed on 23 February 2022).

**Acknowledgments:** The authors would like to thank Gabriele E. Schaumann for her organizational support as a group leader.

**Conflicts of Interest:** The authors declare no conflict of interest.

## Abbreviations

| | |
|---|---|
| n-$TiO_2$ | $TiO_2$ nanoparticles |
| n-$TiO_2$ ⊂ sunscreen (X) | $TiO_2$ nanoparticles extracted from sunscreen (X: sunscreen's ID). |
| X-Y | n-$TiO_2$ ⊂ sunscreen (X) (applied for simplicity in the figures)<br>(X: sunscreen's ID, Y: number of replicates in ToF-SIMS) |
| FX-Y | $TiO_2$ nanoparticles extracted from sunscreen exposed to fulvic acids<br>(F: fulvic acids, X: sunscreen's ID, Y: number of replicates in ToF-SIMS) |

## References

1. Slomberg, D.L.; Catalano, R.; Bartolomei, V.; Labille, J. Release and fate of nanoparticulate $TiO_2$ UV filters from sunscreen: Effects of particle coating and formulation type. *Environ. Pollut.* **2021**, *271*, 116263. [CrossRef] [PubMed]
2. Botta, C.; Labille, J.; Auffan, M.; Borschneck, D.; Miche, H.; Cabié, M.; Masion, A.; Rose, J.; Bottero, J.-Y. $TiO_2$-based nanoparticles released in water from commercialized sunscreens in a life-cycle perspective: Structures and quantities. *Environ. Pollut.* **2011**, *159*, 1543–1550. [CrossRef] [PubMed]
3. Smijs, T.G.; Pavel, S. Titanium dioxide and zinc oxide nanoparticles in sunscreens: Focus on their safety and effectiveness. *Nanotechnol. Sci. Appl.* **2011**, *4*, 95. [CrossRef]
4. Schneider, S.L.; Lim, H.W. A review of inorganic UV filters zinc oxide and titanium dioxide. *Photodermatol. Photoimmunol. Photomed.* **2019**, *35*, 442–446. [CrossRef] [PubMed]
5. Beasley, D.G.; Meyer, T.A. Characterization of the UVA protection provided by avobenzone, zinc oxide, and titanium dioxide in broad-spectrum sunscreen products. *Am. J. Clin. Dermatol.* **2010**, *11*, 413–421. [CrossRef]
6. Gondikas, A.P.; von der Kammer, F.; Reed, R.B.; Wagner, S.; Ranville, J.F.; Hofmann, T. Release of $TiO_2$ nanoparticles from sunscreens into surface waters: A one-year survey at the old Danube recreational Lake. *Environ. Sci. Technol.* **2014**, *48*, 5415–5422. [CrossRef]
7. Meyer, N.; Schafft, M.; Wegner, B.; Wolter, C.; Arlinghaus, R.; Venohr, M.; von Oheimb, G. A day on the shore: Ecological impacts of non-motorised recreational activities in and around inland water bodies. *J. Nat. Conserv.* **2021**, *64*, 126073. [CrossRef]
8. Sánchez-Quiles, D.; Tovar-Sánchez, A. Are sunscreens a new environmental risk associated with coastal tourism? *Environ. Int.* **2015**, *83*, 158–170. [CrossRef]
9. Li, M.; Yin, J.-J.; Wamer, W.G.; Lo, Y.M. Mechanistic characterization of titanium dioxide nanoparticle-induced toxicity using electron spin resonance. *J. Food Drug Anal.* **2014**, *22*, 76–85. [CrossRef]
10. Li, F.; Liang, Z.; Zheng, X.; Zhao, W.; Wu, M.; Wang, Z. Toxicity of nano-$TiO_2$ on algae and the site of reactive oxygen species production. *Aquat. Toxicol.* **2015**, *158*, 1–13. [CrossRef]
11. Brunelli, A.; Pojana, G.; Callegaro, S.; Marcomini, A. Agglomeration and sedimentation of titanium dioxide nanoparticles (n-$TiO_2$) in synthetic and real waters. *J. Nanopart. Res.* **2013**, *15*, 1684. [CrossRef]
12. Sanches, M.V.; Oliva, M.; De Marchi, L.; Cuccaro, A.; Puppi, D.; Chiellini, F.; Freitas, R.; Pretti, C. Ecotoxicological screening of UV-filters using a battery of marine bioassays. *Environ. Pollut.* **2021**, *290*, 118011. [CrossRef] [PubMed]
13. Pettibone, J.M.; Cwiertny, D.M.; Scherer, M.; Grassian, V.H. Adsorption of organic acids on $TiO_2$ nanoparticles: Effects of pH, nanoparticle size, and nanoparticle aggregation. *Langmuir* **2008**, *24*, 6659–6667. [CrossRef] [PubMed]
14. Petosa, A.R.; Jaisi, D.P.; Quevedo, I.R.; Elimelech, M.; Tufenkji, N. Aggregation and deposition of engineered nanomaterials in aquatic environments: Role of physicochemical interactions. *Environ. Sci. Technol.* **2010**, *44*, 6532–6549. [CrossRef] [PubMed]
15. Baalousha, M.; Afshinnia, K.; Guo, L. Natural organic matter composition determines the molecular nature of silver nanomaterial-NOM corona. *Environ. Sci. Nano* **2018**, *5*, 868–881. [CrossRef]

16. Heilgeist, S.; Sekine, R.; Sahin, O.; Stewart, R.A. Finding Nano: Challenges Involved in Monitoring the Presence and Fate of Engineered Titanium Dioxide Nanoparticles in Aquatic Environments. *Water* **2021**, *13*, 734. [CrossRef]
17. Buffle, J. Les substances humiques et leurs interactions avec les ions minéraux. In *Conference Proccedings de la Commission d'Hydrologie Appliquée de l'A.G.H.T.M.*; l'Université d'Orsay: Orsay, France, 1977; pp. 3–10.
18. Lee, S.S.; Fenter, P.; Park, C.; Nagy, K.L. Fulvic acid sorption on muscovite mica as a function of pH and time using in situ X-ray reflectivity. *Langmuir* **2008**, *24*, 7817–7829. [CrossRef]
19. Schumacher, M.; Christl, I.; Vogt, R.D.; Barmettler, K.; Jacobsen, C.; Kretzschmar, R. Chemical composition of aquatic dissolved organic matter in five boreal forest catchments sampled in spring and fall seasons. *Biogeochemistry* **2006**, *80*, 263–275. [CrossRef]
20. Buffle, J.; Mota, A.; Goncalves, M.S. Adsorption of fulvic-like organic ligands and their Cd and Pb complexes at a mercury electrode. *J. Electroanal. Chem. Interfacial Electrochem.* **1987**, *223*, 235–262. [CrossRef]
21. Tayyebi Sabet Khomami, N.; Philippe, A.; Lechtenfeld, O.J.; Guigner, J.-M.; Heissler, S.; Schaumann, G.E. Validation of a field deployable reactor for in situ formation of NOM-engineered nanoparticle corona. *Environ. Sci. Nano* **2020**, *7*, 486–500. [CrossRef]
22. Yu, S.; Liu, J.; Yin, Y.; Shen, M. Interactions between engineered nanoparticles and dissolved organic matter: A review on mechanisms and environmental effects. *J. Environ. Sci.* **2018**, *63*, 198–217. [CrossRef]
23. Danielsson, K.; Gallego-Urrea, J.A.; Hassellov, M.; Gustafsson, S.; Jonsson, C.M. Influence of organic molecules on the aggregation of $TiO_2$ nanoparticles in acidic conditions. *J. Nanopart. Res.* **2017**, *19*, 133. [CrossRef] [PubMed]
24. Louie, S.M.; Tilton, R.D.; Lowry, G.V. Critical review: Impacts of macromolecular coatings on critical physicochemical processes controlling environmental fate of nanomaterials. *Environ. Sci. Nano* **2016**, *3*, 283–310. [CrossRef]
25. Luo, M.; Huang, Y.; Zhu, M.; Tang, Y.; Ren, T.; Ren, J.; Wang, H.; Li, F. Properties of different natural organic matter influence the adsorption and aggregation behavior of $TiO_2$ nanoparticles. *J. Saudi Chem. Soc.* **2018**, *22*, 146–154. [CrossRef]
26. Wang, P. Aggregation of $TiO_2$ nanoparticles in aqueous media: Effects of pH, Ferric Ion and Humic Acid. *Int. J. Environ. Sci. Nat. Resour.* **2017**, *1*, 157–162. [CrossRef]
27. Zhang, Y.; Chen, Y.; Westerhoff, P.; Crittenden, J. Impact of natural organic matter and divalent cations on the stability of aqueous nanoparticles. *Water Res.* **2009**, *43*, 4249–4257. [CrossRef]
28. Tayyebi sabet Khomami, N.; Patel, P.M.; Jusi, C.P.; Trouillet, V.; David, J.; Schaumann, G.E.; Philippe, A. Influential parameters of surface waters on the formation of coating on $TiO_2$ nanoparticles under natural conditions. *Environ. Sci. Nano* **2021**, *8*, 3153–3166. [CrossRef]
29. Mwaanga, P.; Carraway, E.R.; Schlautman, M.A. Preferential sorption of some natural organic matter fractions to titanium dioxide nanoparticles: Influence of pH and ionic strength. *Environ. Monit. Assess.* **2014**, *186*, 8833–8844. [CrossRef] [PubMed]
30. Kim, J.; Shan, W.; Davies, S.H.R.; Baumann, M.J.; Masten, S.J.; Tarabara, V.V. Interactions of aqueous NOM with nanoscale $TiO_2$: Implications for ceramic membrane filtration-ozonation hybrid process. *Environ. Sci. Technol.* **2009**, *43*, 5488–5494. [CrossRef]
31. Drosos, M.; Ren, M.; Frimmel, F.H. The effect of NOM to $TiO_2$: Interactions and photocatalytic behavior. *Appl. Catal. B Environ.* **2015**, *165*, 328–334. [CrossRef]
32. Jayalath, S.; Wu, H.; Larsen, S.C.; Grassian, V.H. Surface adsorption of Suwannee River humic acid on $TiO_2$ nanoparticles: A study of pH and particle size. *Langmuir* **2018**, *34*, 3136–3145. [CrossRef] [PubMed]
33. Slomberg, D.L.; Catalano, R.; Ziarelli, F.; Viel, S.; Bartolomei, V.; Labille, J.; Masion, A. Aqueous aging of a silica coated $TiO_2$ UV filter used in sunscreens: Investigations at the molecular scale with dynamic nuclear polarization NMR. *RSC Adv.* **2020**, *10*, 8266–8274. [CrossRef]
34. Labille, J.; Feng, J.; Botta, C.; Borschneck, D.; Sammut, M.; Cabie, M.; Auffan, M.; Rose, J.; Bottero, J.-Y. Aging of $TiO_2$ nanocomposites used in sunscreen. Dispersion and fate of the degradation products in aqueous environment. *Environ. Pollut.* **2010**, *158*, 3482–3489. [CrossRef] [PubMed]
35. Nickel, C.; Hellack, B.; Nogowski, A.; Babick, F.; Stintz, M.; Maes, H.; Schäffer, A.; Kuhlbusch, T. *Mobility, Fate and Behavior of $TiO_2$ Nanomaterials in Different Environmental Media. Environmental Research of the Federal Ministry for the Environment*; Federal Environment Agency: Dessau-Roßlau, Germany, 2012.
36. Philippe, A.; Schaumann, G.E. Interactions of dissolved organic matter with natural and engineered inorganic colloids: A review. *Environ. Sci. Technol.* **2014**, *48*, 8946–8962. [CrossRef]
37. Nebbioso, A.; Piccolo, A. Molecular characterization of dissolved organic matter (DOM): A critical review. *Anal. Bioanal. Chem.* **2013**, *405*, 109–124. [CrossRef]
38. Galindo, C.; Del Nero, M. Molecular level description of the sorptive fractionation of a fulvic acid on aluminum oxide using electrospray ionization Fourier transform mass spectrometry. *Environ. Sci. Technol.* **2014**, *48*, 7401–7408. [CrossRef]
39. Baer, D.R.; Gaspar, D.J.; Nachimuthu, P.; Techane, S.D.; Castner, D.G. Application of surface chemical analysis tools for characterization of nanoparticles. *Anal. Bioanal. Chem.* **2010**, *396*, 983–1002. [CrossRef]
40. Laboratory for ToF-SIMS Analysis. Available online: https://www.tascon.eu/en/tof-sims.html (accessed on 10 October 2021).
41. Neunzehn, J.; Draude, F.; Golla-Schindler, U.; Arlinghaus, H.F.; Wiesmann, H.-P. Detection of protein coatings on nanoparticles surfaces by ToF-SIMS and advanced electron microscopy. *Surf. Interface Anal.* **2013**, *45*, 1340–1346. [CrossRef]
42. Kulkarni, M.; Mazare, A.; Park, J.; Gongadze, E.; Killian, M.S.; Kralj, S.; von der Mark, K.; Iglic, A.; Schmuki, P. Protein interactions with layers of $TiO_2$ nanotube and nanopore arrays: Morphology and surface charge influence. *Acta Biomater.* **2016**, *45*, 357–366. [CrossRef]

43. Stepien, M.; Saarinen, J.J.; Teisala, H.; Tuominen, M.; Aromaa, M.; Haapanen, J.; Kuusipalo, J.; Makela, J.M.; Toivakka, M. ToF-SIMS analysis of UV-switchable $TiO_2$-nanoparticle-coated paper surface. *Langmuir* **2013**, *29*, 3780–3790. [CrossRef]
44. De Bruycker, K.; Welle, A.; Hirth, S.; Blanksby, S.J.; Barner-Kowollik, C. Mass spectrometry as a tool to advance polymer science. *Nat. Rev. Chem.* **2020**, *4*, 257–268. [CrossRef]
45. Mezger, S.T.; Mingels, A.; Bekers, O.; Cillero-Pastor, B.; Heeren, R. Trends in mass spectrometry imaging for cardiovascular diseases. *Anal. Bioanal. Chem.* **2019**, *411*, 3709–3720. [CrossRef] [PubMed]
46. Su, H.; Li, X.; Huang, L.; Cao, J.; Zhang, M.; Vedarethinam, V.; Di, W.; Hu, Z.; Qian, K. Plasmonic alloys reveal a distinct metabolic phenotype of early gastric cancer. *Adv. Mater.* **2021**, *33*, 2007978. [CrossRef] [PubMed]
47. Aoyagi, S.; Fujiwara, Y.; Takano, A.; Vorng, J.-L.; Gilmore, I.S.; Wang, Y.-C.; Tallarek, E.; Hagenhoff, B.; Iida, S.; Luch, A. Others Evaluation of time-of-flight secondary ion mass spectrometry spectra of peptides by random forest with amino acid labels: Results from a versailles project on advanced materials and standards interlaboratory study. *Anal. Chem.* **2021**, *93*, 4191–4197. [CrossRef]
48. Zhang, M.; Huang, L.; Yang, J.; Xu, W.; Su, H.; Cao, J.; Wang, Q.; Pu, J.; Qian, K. Ultra-Fast Label-Free Serum Metabolic Diagnosis of Coronary Heart Disease via a Deep Stabilizer. *Adv. Sci.* **2021**, *8*, 2101333. [CrossRef]
49. Philippe, A.; Kosik, J.; Welle, A.; Guigner, J.-M.; Clemens, O.; Schaumann, G.E. Extraction and characterization methods for titanium dioxide nanoparticles from commercialized sunscreens. *Environ. Sci. Nano* **2018**, *5*, 191–202. [CrossRef]
50. Metreveli, G.; Philippe, A.; Schaumann, G.E. Disaggregation of silver nanoparticle homoaggregates in a river water matrix. *Sci. Total Environ.* **2015**, *535*, 35–44. [CrossRef]
51. Wilkin, G.A.; Huang, X. K-means clustering algorithms: Implementation and comparison. In Proceedings of the Second International Multi-Symposiums on Computer and Computational Sciences (IMSCCS 2007), Iowa City, IA, 13–15 August 2007; pp. 133–136.
52. Abbas, O.A. Comparisons between data clustering algorithms. *Int. Arab. J. Inf. Technol. IAJIT* **2008**, *5*, 320–325.
53. K-Means Clustering-Deciding How Many Clusters to Build. Available online: https://blog.exploratory.io/k-means-clustering-deciding-how-many-clusters-to-build-d33fd9c68088 (accessed on 5 January 2022).
54. Lovatti, B.P.; Nascimento, M.H.; Neto, Á.C.; Castro, E.V.; Filgueiras, P.R. Use of Random forest in the identification of important variables. *Microchem. J.* **2019**, *145*, 1129–1134. [CrossRef]
55. Biau, G.; Scornet, E. A random forest guided tour. *Test* **2016**, *25*, 197–227. [CrossRef]
56. Scornet, E. Trees, Forests, and Impurity-Based Variable Importance. *arXiv* **2020**, arXiv:2001.04295v2.
57. Yu, H.; Song, Y.; Liu, R.; Xi, B.; Du, E.; Xiao, S. Variation of dissolved fulvic acid from wetland measured by UV spectrum deconvolution and fluorescence excitation-emission matrix spectrum with self-organizing map. *J. Soils Sediments* **2014**, *14*, 1088–1097. [CrossRef]
58. Everitt, B.S.; Landau, S.; Leese, M.; Stahl, D. *Cluster Analysis*; John Wiley & Sons: Hoboken, NJ, USA, 2011; p. 330.
59. Havelund, R.; Seah, M.P.; Shard, A.G.; Gilmore, I.S. Electron flood gun damage effects in 3D secondary ion mass spectrometry imaging of organics. *J. Am. Soc. Mass Spectrom.* **2014**, *25*, 1565–1571. [CrossRef] [PubMed]
60. Patiny, L.; Borel, A. ChemCalc: A building block for tomorrow's chemical infrastructure. *J. Chem. Inf. Model.* **2013**, *53*, 1223–1228. [CrossRef] [PubMed]